Lattice Boltzmann simulations of the time-averaged forces on a cylinder in a sound field

2005 J. Phys. A: Math. Gen. 38 3265

(http://iopscience.iop.org/0305-4470/38/15/003)

INSTITUTE OF PHYSICS PUBLISHING JOURNAL OF PHYSICS A: MATHEMATICAL AND GENERAL

J. Phys. A: Math. Gen. **38** (2005) 3265–3277 doi:10.1088/0305-4470/38/15/003

Lattice Boltzmann simulations of the time-averaged forces on a cylinder in a sound field

David Haydock

Unilever R&D Colworth, Sharnbrook, Bedford MK44 1LQ, UK
and
Department of Physics, Theoretical Physics, University of Oxford, 1 Keble Road, Oxford OX1 3NP, UK

Received 30 November 2004
Published 30 March 2005
Online at stacks.iop.org/JPhysA/38/3265

Abstract

We show that lattice Boltzmann simulations can be used to model the radiation force on an object in a standing wave acoustic field and comparisons are made to theoretical predictions. We show how viscous effects change the radiation force and predict the motion of a particle placed near a boundary where viscous effects are important.

PACS numbers: 43.25.+y, 43.35.+d, 62.60.+v, 05.50.+q

1. Introduction

The radiation force on an object in a sound field is the total time-averaged force on the object in an acoustic field. It is a non-linear effect which is produced by momentum transfer from the wave to the object [1–6].

The radiation force on an object has a number of applications: it can be used to measure the power output from an ultrasonic transducer [7]. It is used in ultrasonic levitation to suspend droplets in air to study effects such as heat transfer [8, 9]. It is also being studied in microfluidic applications to manipulate particle so that a higher concentration can be achieved over any sensors or active areas [10, 11]. The reasons behind this behaviour are unclear, and to understand and control the particle motion, it is important to better characterize the time-averaged force. For a few simple systems, the time-averaged force has been determined analytically. However, for more complex systems, analytical solutions are likely to prove difficult, so modelling methodologies need to be found. The aim of this paper is to describe one such approach, a lattice Boltzmann simulation, which can predict the radiation force from a direct solution of the Navier–Stokes equations.

For a rigid object which is not deformed by the sound field, the radiation force is produced by the time-averaged pressure [12], the drag on the object due to acoustic streaming [12] and

a component due to any harmonic movement of the object in the sound field [13]. For small objects, much smaller than the wavelength, in a standing wave field the radiation force pushes the object towards either the pressure or velocity anti-node depending on the density and compressibility of the object.

Conventionally, the acoustic boundary layer thickness β^{-1} is assumed to be small compared to the dimensions of any particle or object, where $\beta^{-1} = \sqrt{2\nu/\omega}$, ν is the kinamatic viscosity of the fluid, and ω is the angular frequency of the wave. Here the solution is greatly simplified by assuming the fluid is inviscid and the viscous effects such as streaming can be neglected [12, 14]. There are, however, a number of applications where this assumption is typically violated, for example in microfluidics. In these cases viscous effects such as streaming must be included [14].

King was one of the first to analyse the radiation force [4]. He published a landmark paper describing the radiation force on a sphere due to wave propagation in an inviscid fluid. He derived a formula for the second-order pressure and calculated the radiation force due to a standing wave and a travelling wave. Most studies presented have only considered spherical objects, but there have been a few investigations into the radiation force on a cylinder. These considered an inviscid fluid where the cylinder is free to move in the acoustic field. Awatani was probably the first to calculate the radiation force on a cylinder in 1954 [15]. He presented calculations for the variation in the force on a rigid cylinder due to a travelling wave field. He also claimed to have calculated the radiation force for a standing wave but on inspection the wave propagates in the x-direction. In 1988 and 1993 Hasegawa *et al* [16, 17] published calculations for elastic cylinder spherical shells and cylindrical shells in a travelling wave field. In 1990 Wu *et al* also produced an analytical study which was compared to experimental results [18]. They found an agreement to within 20%, but their calculation was for two incident waves rather than an incident and scattered wave. Ebenezer and Stepanishen presented two papers using numerical solutions to the radiation force for a cylinder that is vibrating at an arbitrary number of natural frequencies [19, 20]. In 2004 Townsend *et al* used the ODE solver within MATLAB to calculate the position of particles subject to a standing wave and steady laminar flow not induced by the sound wave [21]. In 2004 Cosgrove *et al* [22] simulated the motion of particles in a sound field using lattice Boltzmann simulations and compared the results to the predictions by Wu [18]. However, the Wu theory does not accurately model a particle in a standing wave [23] and their results appear to show significant deviations from the theoretical predictions. They also do not consider the effects of acoustic streaming.

Recently, Haydock and Yeomans [23–25] used a lattice Boltzmann algorithm to model acoustic streaming. Both the radiation force and acoustic streaming are essentially produced by the same mechanism: a time-averaged momentum transfer from the wave. For acoustic streaming the momentum transfer is to the fluid, and generally produces a steady flow, whereas for the radiation force the momentum transfer leads to a time-averaged force on an object [1, 3–6, 26]. Here we compare lattice Boltzmann simulations to a more accurate theory than that used by Cosgrove *et al* for a standing wave, and we consider the effects of viscosity and the size of the simulation when making the comparison. We show that it can be used to predict both the time-averaged force and motion for complicated systems, where analytical investigations are not possible, and where viscous effects, such as acoustic streaming, cannot be ignored. This work formed part of a DPhil thesis [23].

In the next section we introduce the lattice Boltzmann approach. In section 3 we compare the simulation results with theoretical predictions for a cylinder fixed in space. In section 4 we consider the motion of a cylinder free to move in the standing wave acoustic field. In section 5 we present our concluding comments.

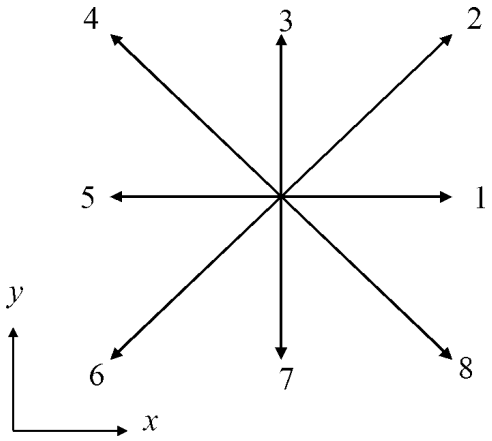

Figure 1. Lattice vectors for the lattice Boltzmann model.

2. The lattice Boltzmann algorithm

The lattice Boltzmann model we use is the single-relaxation-time Bhatnagar–Gross–Krook (BGK) scheme on a two-dimensional square lattice [27]. Lattice vectors are

$$\mathbf{e}_i = \left(\cos\left\{\tfrac{1}{4}\pi(i-1)\right\}, \sin\left\{\tfrac{1}{4}\pi(i-1)\right\}\right), \qquad i = 1, 3, 5, 7$$
$$\mathbf{e}_i = \left(\sqrt{2}\cos\left\{\tfrac{1}{4}\pi(i-1)\right\}, \sqrt{2}\sin\left\{\tfrac{1}{4}\pi(i-1)\right\}\right), \qquad i = 2, 4, 6, 8$$

together with a zero velocity vector $\mathbf{e}_0 = (0, 0)$ as shown in figure 1. A set of partial densities, $f_i(\mathbf{x}, t)$, associated with each lattice direction i are defined on each lattice site $\mathbf{x}$. These are related to the physical variables, density $\rho(\mathbf{x}, t)$, and velocity $\mathbf{u}(\mathbf{x}, t)$ by

$$\sum_i f_i(\mathbf{x}, t) = \rho(\mathbf{x}, t), \qquad \sum_i f_i(\mathbf{x}, t)\mathbf{e}_i = \rho(\mathbf{x}, t)\mathbf{u}(\mathbf{x}, t). \tag{1}$$

The partial densities evolve with time t according to

$$f_i(\mathbf{x} + \mathbf{e}_i, t + 1) - f_i(\mathbf{x}, t) = \frac{1}{\tau}\left(f_i - f_i^0\right) \tag{2}$$

where the local equilibrium distributions are

$$f_i^0 = \rho w_i\left\{1 + 3\mathbf{e}_i \cdot \mathbf{u} + \tfrac{9}{2}(\mathbf{e}_i \cdot \mathbf{u})^2 - \tfrac{3}{2}u^2\right\}, \qquad i = 1, 2, \ldots, 8, \tag{3}$$

with $w_1 = w_3 = w_5 = w_7 = 1/9$ and $w_2 = w_4 = w_6 = w_8 = 36$ and

$$f_0^0 = \rho\left\{\tfrac{4}{9} - \tfrac{2}{3}u^2\right\}. \tag{4}$$

In equation (2), the left-hand side corresponds to the propagation step, where momentum is transferred, and the right-hand side represents the relaxation process which determines the viscous properties of the fluid. In the continuum limit a Chapman–Enskog expansion of the numerical scheme reproduces the Navier–Stokes equations [27]:

$$\partial_t \rho + \partial_\alpha \rho u_\alpha = 0 \tag{5}$$
$$\partial_t \rho u_\beta + u_\beta \partial_\alpha \rho u_\alpha + \rho u_\alpha \partial_\alpha u_\beta = -\partial_\alpha P + \rho\nu\partial_\alpha[\partial_\beta u_\alpha + \partial_\alpha u_\beta] \tag{6}$$

with pressure $P = \rho/3$, kinematic viscosity $\nu = (2\tau - 1)/6$ and speed of sound $c_0 = 1/\sqrt{3}$.

The boundary conditions used for non-slip walls was the bounce back boundary condition [28] as used in our previous simulations [23–25]. For the particle we use the Ladd moving boundary conditions [29].

Table 1. Parameters used in lattice Boltzmann simulations of the radiation force on a fixed cylinder. L_x and L_y are the dimensions of the simulation in the x and y directions respectively, λ is the wavelength, h is the distance from the acoustic source, a is the radius of the cylinder, τ is the relaxation time, ω is the angular frequency and ν is the kinematic viscosity.

$L_x = \lambda$	L_y	h	a	τ	ω	ν
1000	100	375	5	1	0.0036	0.167
1000	100	375	10	1	0.0036	0.167
1000	200	375	20	1	0.0036	0.167
1000	200	375	40	1	0.0036	0.167
1000	500	375	80	1	0.0036	0.167
500	100	186	10	1	0.0073	0.167
200	100	75	10	1	0.0182	0.167
1000	100	375	10	0.502	0.0036	0.000 67
1000	100	375	10	0.52	0.0036	0.006 67
1000	100	375	10	0.8	0.0036	0.1

3. Radiation force on a fixed cylinder

We first consider a rigid cylinder which is fixed in space. This allows us to compare the simulated radiation force with the theoretical predictions without the added complexity of considering the motion of the particle. We use the inviscid theory developed by Haydock [30].

3.1. Choice of parameters

We now describe the choice of parameters used to simulate the radiation force on a fixed cylinder. The theory we use is for an inviscid fluid which is valid when $\beta^{-1} \ll a$ [14].

The choice of parameters will inevitably be a compromise as $(\beta a)^{-1} \to 0$. Lattice effects become more important as $\nu \to 0$. This reduces the accuracy of the lattice approximation of a cylinder [23]. $a \to \infty$ requires a compromise between the computational cost through increasing the size of the lattice, and boundary effects. ω is also constrained because we require that $\lambda \gg a$ so that the force changes with position (the force varies with period 2ω) and to minimize any errors due to the rapid change in velocity potential at the cylinder boundary.

Therefore, we consider simulations of length $L_x = \lambda$, and width L_y with the properties detailed in table 1. In each case the particle was placed at a maximum in the radiation force ($h = 3\lambda/8$) where h is the distance from the acoustic source. These parameters allow us to assess how the simulated radiation force and theoretical prediction converge as $(\beta a)^{-1} \to 0$. They also allow us to determine how changes in the viscous effects due to changes in a, λ and τ affect the radiation force.

We consider a standing wave acoustic field with periodic boundary conditions at all boundaries. The wave is initialized as $\rho = \rho_0 + \Delta\rho_1 \cos(kx)$, $\mathbf{u} = 0$, $\Delta\rho_1 = 0.01$ and maintained by setting the partial densities at $x = 0$ to the equilibrium distribution function (3) and (4) with $\rho = \rho_0 + \Delta\rho_1 \cos(\omega t)$ [23–25].

3.2. Effect of particle radius, wavelength and viscosity on the radiation force

Details of the comparison between the simulations and theoretical predictions of the radiation force are given in table 2 for the variation in force with particle radius, table 3 for the variation in force with viscosity and table 4 for the variation in force with wavelength. The variation in the percentage difference in the radiation force between the theory and simulations with

Table 2. Effect of particle size on the radiation force. $\lambda = 1000$, $\tau = 1$, $\nu = 0.167$. F_{th}: theoretical radiation force, F_{LB}: simulation radiation force.

a	$(\beta a)^{-1}$	F_{th} (10^{-5})	F_{LB} (10^{-5})	Difference (10^{-5})	Difference (%)
5	1.9	−1.24	−3.04	−1.81	146
10	0.96	−4.95	−8.2	−3.26	66
20	0.48	−19.79	−25.12	−5.33	27
40	0.24	−77.85	−81.02	−3.18	4
80	0.12	−265.7	−247.2	18.4	−6.9

Table 3. Effect of viscosity on the radiation force. $a = 10$, $\lambda = 1000$. F_{th}: theoretical radiation force, F_{LB}: simulation radiation force.

T	ν	$(\beta a)^{-1}$	F_{th} (10^{-5})	F_{LB} (10^{-5})	Difference (10^{-5})	Difference (%)
1	0.167	0.97	−4.95	−8.2	3.26	66
0.8	0.1	0.75	−4.95	−7.66	2.71	55
0.52	0.006 67	0.19	−4.95	−5.9	−0.98	20
0.502	0.000 67	0.06	−4.95	−5.49	−0.54	11

Table 4. Effect of wavelength on the radiation force. $a = 10$, $\tau = 1$, $\nu = 0.167$. F_{th}: theoretical radiation force, F_{LB}: simulation radiation force.

λ	$(\beta a)^{-1}$	F_{th} (10^{-5})	F_{LB} (10^{-5})	Difference (10^{-5})	Difference (%)
1000	0.96	−4.95	−8.2	−3.26	66
500	0.68	−9.9	−13.5	−3.6	36
200	0.43	−23.77	−24.4	−0.6	2.7

$(\beta a)^{-1}$ is shown in figure 2. We emphasize that we do not expect exact agreement with the theory since the simulations necessarily contain viscous contributions to the radiation force and attenuation of the acoustic wave, and the theory itself is not exact.

Consider first table 2. We set $\nu = 0.167$, $\lambda = 1000$ and vary the particle radius a from 5 to 80. This corresponds to values of $(\beta a)^{-1}$ from 1.9 to 0.12. As $(\beta a)^{-1}$ reduces the simulated force approaches the theoretical result, but there is a small overshoot for the largest radius considered. This may be due to spurious boundary effects as the particle radius becomes large, approaching the size of the simulation box. To investigate this figure 3 ($\lambda = 1000$, $\nu = 0.167$, $a = 80$) shows the density variation of the fluid for the largest radius considered. The distortion in the first-order wave created by the largest particle does appear to reach the boundary confirming that a larger simulation is required. However, there are other possible causes for the overshoot: for example, the approximations in the theory assumes $\lambda \gg a$. This could lead to an overprediction of the radiation force.

In table 3 we present results for $a = 10$, $\lambda = 1000$, and variations in viscosity from 0.167 to 0.000 67. This corresponds to values of $(\beta a)^{-1}$ from 0.97 to 0.06. The percentage difference between the theory and simulation decreases smoothly as $(\beta a)^{-1} \to 0$. However, as the viscosity is lowered errors due to finite lattice effects will become more pronounced, so we do not expect exact agreement as $(\beta a)^{-1} \to 0$.

In table 4 we present the results for $a = 10$, $\nu = 0.167$, and variations in wavelength from 1000 to 200. This corresponds to values of $(\beta a)^{-1}$ from 0.96 to 0.43. The percentage difference between theory again reduces as $(\beta a)^{-1}$ reduces, but looks as though it will significantly

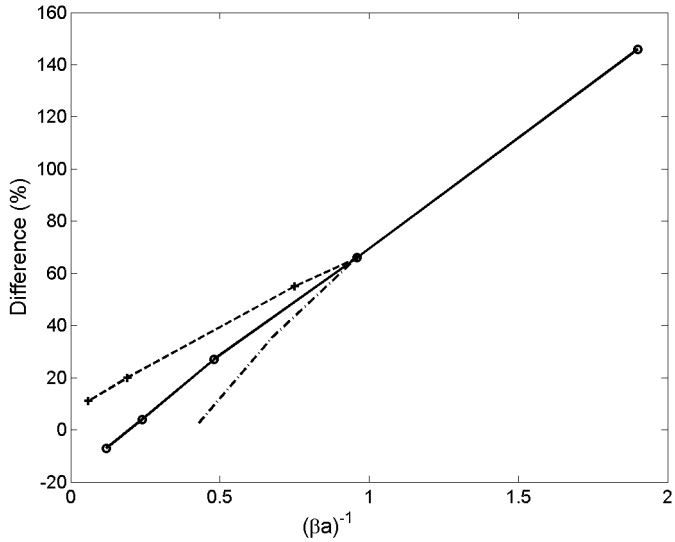

Figure 2. Percentage difference in radiation force between theory and the simulations as a function of $(\beta a)^{-1}$. Solid line (○): changing the particle radius a, (+) dashed line: changing the viscosity, (∗) dashed and dotted line: changing the wavelength.

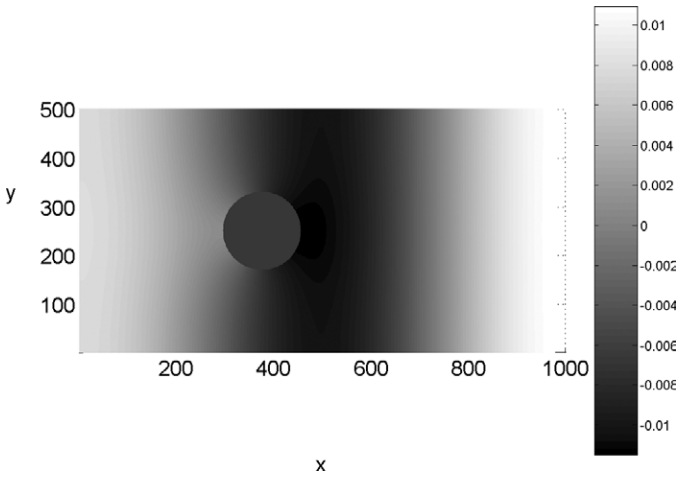

Figure 3. First-order density variation ($\tau = 1, L_x = 1000, L_y = 500, a = 80, h = 375$). Black: low density through to white: high density.

overshoot as $(\beta a)^{-1} \to 0$. However, the theory assumes that $ka \ll kh$ which will not be true when $\lambda \to a$, so the theory will not be accurate as $(\beta a)^{-1} \to 0$ through changing the wavelength. We note for $(\beta a)^{-1} = 0.43$ that the theoretical and simulated results are almost equal. We believe that this is a result of a coincidental balance of viscous effects. These will be explained shortly.

As we increase $(\beta a)^{-1}$ the viscous effects become more important [14], which will lead to a discrepancy between the model and the theoretical prediction. The inviscid theory considers scattering from the particle. However, in a real viscous fluid, momentum is transferred in the boundary layer [12, 14]. Part of this momentum transfer is converted into acoustic streaming,

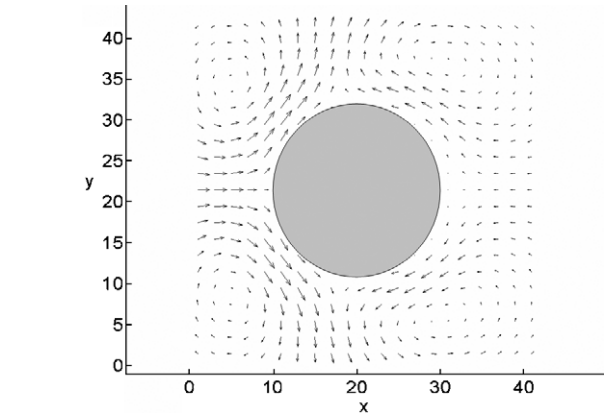

(*a*)

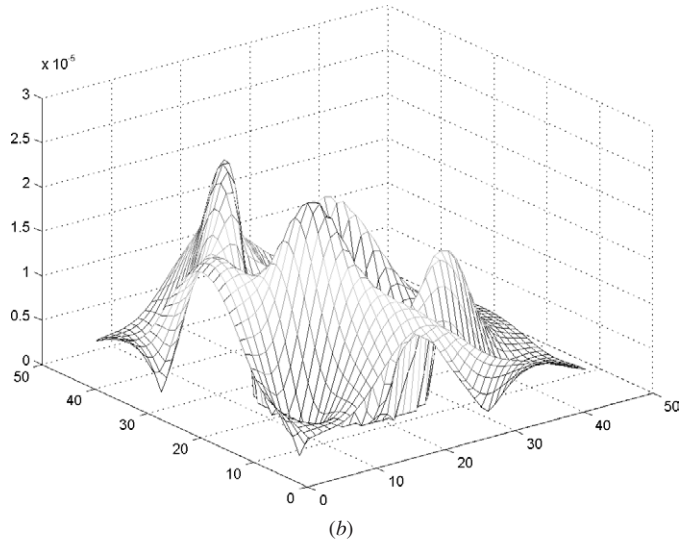

(*b*)

Figure 4. Acoustic streaming velocity around the cylinder for the $L_x = 200$, $L_y = 100$, $\tau = 1$, $a = 10$ simulation. (*a*) Velocity vector plot, (*b*) magnitude of streaming velocity.

and the remainder into a time-averaged pressure [12, 14]. This generally leads to a radiation force which is greater than the inviscid prediction [12, 14]. There can also be a contribution due to acoustic streaming which is created away from the particle [11, 14]. Figure 2 and tables 2 to 4 indeed show that the simulations predict large discrepancies due to the increased viscous contribution to the radiation force. However, the increase is not simply a function of $(\beta a)^{-1}$.

For a standing wave where the particle is positioned away from the nodes or anti-nodes, the field will not be symmetrical about the particle [23]. All the particles in this section are positioned mid-way between a pressure and velocity node ($h = 3\lambda/8$). This can produce a more complex streaming pattern than typically considered in analytical predictions [1].

Consider the streaming field around the particle radius $a = 10$ when $\lambda = 200$ ($\nu = 0.167$, $(\beta a)^{-1} = 0.43$) shown in figure 4. This shows an asymmetric streaming profile which opposes the time-averaged pressure. For this simulation the radiation force is surprisingly close to the

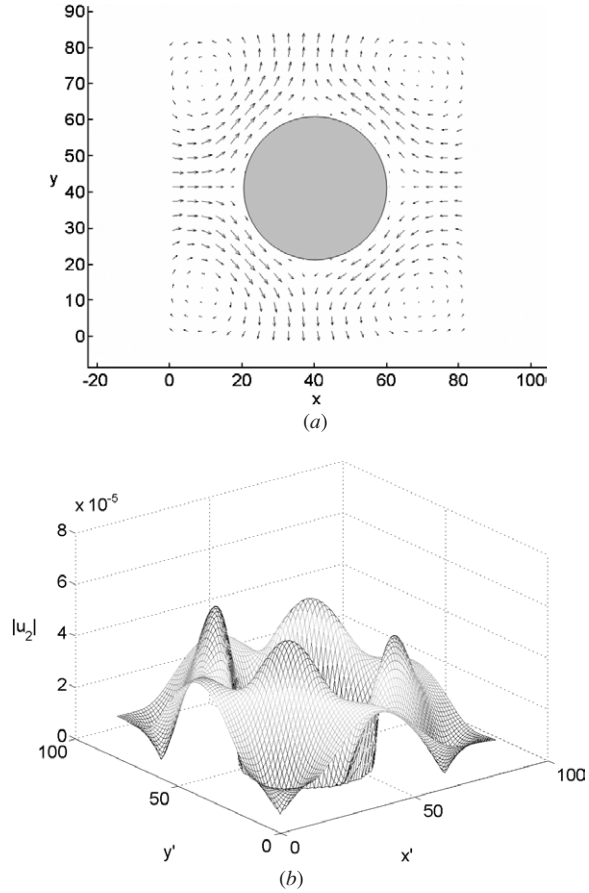

Figure 5. Acoustic streaming velocity around the cylinder for the $L_x = 1000$, $L_y = 200$, $\tau = 1$, $a = 20$ simulation. (*a*) Velocity vector plot, (*b*) magnitude of the streaming velocity.

theoretical prediction for an inviscid fluid (table 4) despite $(\beta a)^{-1}$ being reasonably high. If we now compare this with a simulation with a similar simulation with $(\beta a)^{-1} = 48$ for a particle radius $a = 20$ when $\lambda = 1000$ ($\nu = 0.167$) in table 2, the streaming field (figure 5) is approximately symmetric and we find that the predicted radiation force is higher. This is because the radiation force has not been reduced by the effects of asymmetric acoustic streaming. These effects will make determining radiation force a complicated problem when viscosity is important.

4. The effects of radiation force on a cylinder free to move in the sound field

In the previous section we showed that the lattice Boltzmann scheme can simulate the radiation force on an object. We also showed how viscous effects can add to this force, making analytical predictions very difficult.

In this section we will consider how the radiation force affects the time-averaged motion of a cylinder in a standing wave field. We will first consider the simplest case where the particle is placed in an infinite periodic field so that boundary effects do not need to be considered. For this simulation we can use theoretical predictions to determine how the particle will move.

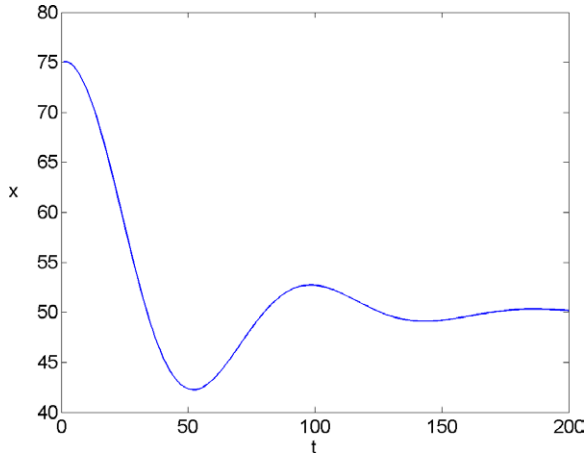

Figure 6. (*a*) Time-averaged particle position, (*b*) time-averaged particle velocity ($L_x = 200$, $L_y = 100$, $\tau = 0.6$, $a = 10$, $\rho_0 = 1$, $\rho_1 = 100$).

We will then simulate a more complex situation where a particle is placed near a boundary in a viscous fluid. This motion would be difficult to predict analytically.

4.1. Periodic boundaries

In this section we will demonstrate that lattice Boltzmann simulations of the radiation force on a free particle produce the motion predicted by theory. Once the particle is free to move we cannot measure the radiation force as this will be balanced by the time-averaged drag force on the particle due to its motion.

We choose the parameters $L_x = \lambda = 200$, $L_y = 100$, $\tau = 0.6$ ($\nu = 0.0333$), $h = 3\lambda/8$, a particle density $\rho_1 = 100$ and a particle radius $a = 10$. This gives $(\beta a)^{-1} = 0.19$, so the viscous effects should be small. We have not included gravitational effects in the simulations, so the particle motion will only be due to the acoustic field. Using the theoretical predictions by Haydock [30] for an inviscid fluid the particle should be forced to the pressure nodes $h = \lambda/4$.

Figure 6 shows the simulation results for the position of the particle in the x-direction, and the particle velocity as a function of time. As expected the particle moves to the pressure node. However, its momentum is sufficiently high that it overshoots the node producing a classic underdamped response. If the mass of the particle is reduced or the viscosity is increased the damping is increased as expected.

4.2. Effects of boundaries

In this section we use the lattice Boltzmann scheme to predict the motion of a particle which is placed close to a boundary in a viscous fluid. We choose a simulation with parameters $L_x = \lambda = 1000$, $L_y = 100$, $\tau = 1$ ($\nu = 0.167$), $a = 5$, and place the particle at $h = 3\lambda/8$ and $l_y = 5$ where l_y is the initial distance from the wall at $y = 0$. We also increase the amplitude of the wave to $\Delta\rho_1 = 0.02$. We expect the time-averaged motion of the particle to be due to a combination of the following forces: the time-averaged pressure described by the inviscid theory, an additional time-averaged pressure due to momentum transfer in the viscous boundary layer, a force due to any local streaming forces generated by the particle and a force due to Rayleigh streaming generated at the boundaries ($y = 0$, $y = L_y$) [1, 14, 23, 24].

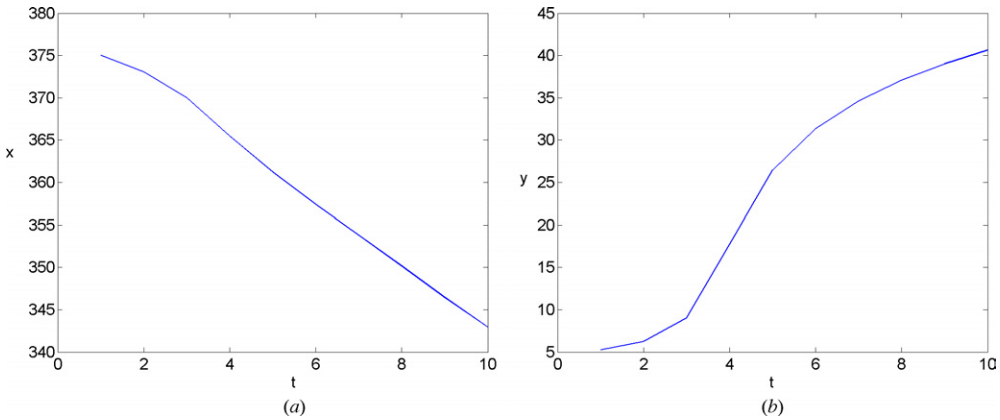

Figure 7. (*a*) Time-averaged x-coordinate of the particle, (*b*) time-averaged y-coordinates of the particle, (*c*) schematic of the time-averaged particle position ($L_x = 1000$, $L_y = 100$, $\tau = 1$, $a = 5$, $\rho_0 = 1$, $\rho_1 = 100$).

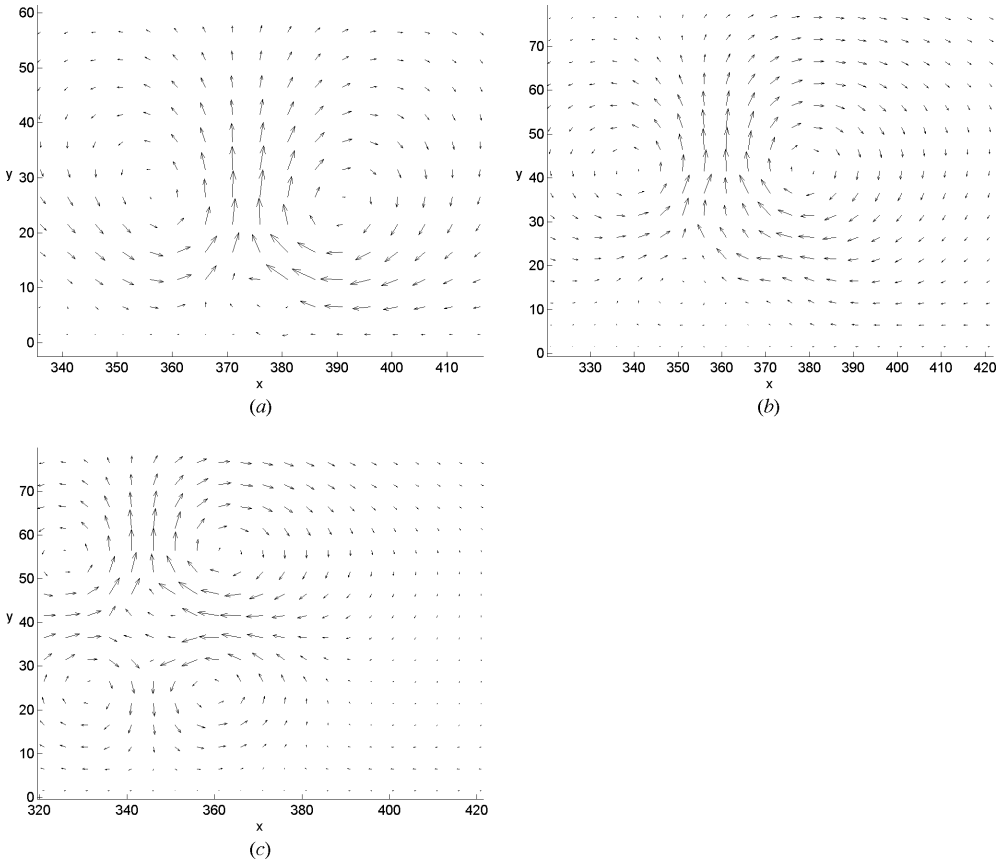

Figure 8. Snapshots of the streaming profile as the particle moves away from the boundary at $y = 0$.

The particle was placed at a maximum of both the inviscid radiation force and the x-component of the expected Rayleigh streaming produced by a standing wave between parallel plates. The time-averaged pressure due to a standing wave without the presence of boundaries would lead to a force which would move the particle from $x = h$ to $x = \lambda/4$ (figure 6). Rayleigh streaming would lead to a time-averaged drag force which would initially move the particle from $x = h$ towards $x = \lambda/2$ and then to the centre of the channel.

Figure 7 shows the particle position as a function of time. The figures show that the particle is unexpectedly driven away from the non-slip boundary, which is not due to either Rayleigh streaming or the radiation force seen without boundaries. To explain this we consider figure 8, a series of time averages of the Lagrangian velocity field as the particle moves away from the surface. Close inspection of the streaming velocities produced in the vicinity of the particle shows that most of the acoustic streaming is due to the interaction of the wave with the particle rather than the plate surface. We see the formation of the typical four-vortex streaming pattern seen around a cylindrical object. However, while the object is close to the boundary only two of the inner vortices are produced. This appears to pull the particle away from the surface. Once the particle has moved from the surface, the additional vortices are produced and the drag force due to streaming appears to be balanced.

5. Relating the models to the real world

To relate the non-dimensional lattice Boltzmann parameters $\mathbf{u}$, $\mathbf{x}$, t, ν and $\mathbf{F}$ to real-world parameters $\mathbf{u}'$, $\mathbf{x}'$, t', ν' and $\mathbf{F}'$, we use a characteristic velocity V and length L of the real system as follows: $u' = Vu$, $x' = Lx$, $t' = (L/V)t$, $\nu' = VL\nu$, $\mathbf{F}' = (\rho V^2/L)\mathbf{F}$, $V = c_0'/c_0$. If we consider a wave propagating in air assuming international standard atmosphere properties at sea level [31] ($c' = 340\ \mathrm{ms}^{-1}$, $\rho_0' = 1.2\ \mathrm{kg\ m}^{-3}$, $\nu' = 1.4 \times 10^{-5}\ \mathrm{m}^2\ \mathrm{s}^{-1}$) and choosing $\nu = 0.167$ then $V = 588.9\ \mathrm{ms}^{-1}$, and $L = 1.43 \times 10^{-7}$. The simulation used to model the boundary effects in section 4.2 has real parameters $f' = 2.4$ MHz, $L_x' = 0.14$ mm, $L_y' = 14.3\ \mu$m, $a' = 0.71\ \mu$m the intensity of the wave $I' = 9.43\ \mathrm{kW\ m}^{-2}$ ($I' = 0.943\ \mathrm{W\ cm}^{-2}$), and each time step represents 0.24 ns.

6. Conclusions

We have shown that the lattice Boltzmann modelling methodology can be used to quantitatively simulate the radiation force on an object in an acoustic field. We have also demonstrated that we can use the Ladd moving boundary conditions to predict the motion of a particle with a density greater than the surrounding fluid.

We have demonstrated that in line with theoretical prediction, the simulations generally show that viscous effects increase the radiation force on an object. However, this is complicated by the acoustic streaming effects which not only reduce the amount of momentum transferred to the time-averaged pressure P_2 but can also reduce the radiation force due to the asymmetric streaming profile that is produced away from the velocity or pressure nodes.

We have shown that the simulations can be used to predict the motion of particles when the geometry is too complicated for analytical theories. We demonstrated this by simulating the motion of a particle placed at a non-slip boundary. The effects of streaming caused the particle to be removed from the surface.

We have not considered the motion of particles which have a density either close to or lower than the surrounding fluid. This may be difficult using the Ladd boundary conditions as they are known to overpredict the density under these conditions.

We believe that it should be relatively easy to extend the methodology to simulate the radiation force on multiple particles. In addition to determining force the boundary conditions also include the effects of torque, so the simulations will automatically include radiation torque effects when shielding between the particles leads to a force which does not act through the centre of mass.

References

[1] Nyborg W L M 1965 Acoustic streaming *Physical Acoustics* vol 2B ed W P Mason and R N Thurston (New York: Academic) pp 265–331

[2] Sato M and Fujii T 2001 Quantum mechanical representation of acoustic streaming and acoustic radiation pressure *Phys. Rev.* E **64** 026311, 1–5

[3] Lighthill J 2001 *Waves in Fluids* (Cambridge: Cambridge University Press) pp 337–51

[4] King L V 1934 On the acoustic radiation pressure on spheres *Proc. R. Soc.* A **147** 212–40

[5] Mitome H 1998 The mechanism of generation of acoustic streaming *Electron. Commun. Japan* Part 3 **81** 1–8

[6] Kamakura T 1999 Unified description of second-order phenomena in sound waves *Electron. Commun. Japan* Part 3 **82** 1648–53

[7] Swamy K M and Keil F J 2002 Ultrasonic power measurement in the milliwatt region by the radiation float method *Ultrason. Sonochem.* **9** 305–10

[8] Trinh E H and Robey J I 1994 Experimental study of streaming flows associated with ultrasonic levitators *Phys. Fluids* **6** 3567–79

[9] Yarin A L, Brenn G, Kastner O, Rensink D and Tropea C 1999 Evaporation of acoustically levitated droplets *J. Fluid Mech.* **399** 151–204

[10] Coakely W T 2003 *Presentation at the Cell Manipulation Science Meeting UMIST (18–19 March)*

[11] Spengler J F, Coakley W T and Christensen K T 2003 Miro-streaming effects on particle concentration in an ultrasonic standing wave *AIChE J.* **49** 2773–82

[12] Westervelt P J 1951 The theory of steady forces caused by sound waves *J. Acoust. Soc. Am.* **23** 312–5

[13] Nyborg W L M 1967 Radiation pressure on a small rigid sphere *J. Acoust. Soc. Am.* **42** 947–51

[14] Danilov S D and Mironov M A 2000 Mean force on a small sphere in a sound field in a viscous fluid *J. Acoust. Soc. Am.* **107** 143–53

[15] Awatani J 1955 Study on acoustic radiation pressure (IV) (radiation pressure on a cylinder) *Mem. Inst. Sci. Osaka Univ.* **12** 95–102

[16] Hasegawa T, Saka K, Inoue N and Matsuzawa K 1988 Acoustic radiation force experienced by a solid cylinder in a plane progressive field *J. Acoust. Soc. Am.* **83** 1770–6

[17] Hasegawa T, Hino Y, Annou A, Noda H, Kato M and Inoue N 1993 Acoustic radiation pressure acting on spherical and cylindrical shells *J. Acoust. Soc. Am.* **93** 154–61

[18] Wu J, Du G, Work S S and Warshaw D M 1990 Acoustic radiation pressure on a rigid cylinder: an analytical theory and experiments *J. Acoust. Soc. Am.* **87** 581–6

[19] Ebenezer D D and Stepanishen P R 1991 Wave-vector-time domain and Kirchoff integral equation methods to determine the transient acoustic radiation loading on circular cylinders *J. Acoust. Soc. Am.* **89** 2532–44

[20] Ebenezer D D and Stepanishen P R 1991 Wave-vector-time domain technique to determine the transient acoustic radiation loading on cylindrical vibrators in an inviscid fluid with axial flow *J. Acoust. Soc. Am.* **89** 39–51

[21] Townsend R J, Hill W, Harris N R and White N M 2004 Modelling of particle paths passing through an ultrasonic standing wave *Ultrasonics* **42** 319–24

[22] Cosgrove J A, Buick J M, Campell D M and Greated C A 2004 Numerical simulations of particle motion in an ultrasound field using the lattice Boltzmann model *Ultrasonics* **43** 21–5

[23] Haydock D 2004 Lattice Boltzmann simulations of acoustic streaming and the radiation force on objects in a sound field *PhD Thesis* University of Oxford

[24] Haydock D and Yeomans J M 2001 Lattice Boltzmann simulations of acoustic streaming *J. Phys. A: Math. Gen.* **34** 5201–13

[25] Haydock D and Yeomans J M 2003 Lattice Boltzmann simulations of attenuation-driven acoustic streaming *J. Phys. A: Math. Gen.* **36** 5683–94

[26] Sato M and Fujii T 2001 Quantum mechanical representation of acoustic streaming and acoustic radiation pressure *Phys. Rev.* E **64** 026311, 1–5

[27] Chen S and Doolen G D 1998 Lattice Boltzmann method for fluid flows *Ann. Rev. Fluid Mech.* **30** 329–64

[28] Rothman D H and Zaleski S 1997 *Lattice Gas Cellular Automata: Simple Models of Complex Hydrodynamics* (Cambridge: Cambridge University Press)

[29] Ladd A J C and Verberg R 2001 Lattice-Boltzmann simulations of particle-fluid suspensions *J. Stat. Phys.* **104** 1191–251

[30] Haydock D 2005 Calculation of the radiation force on a cylinder in a standing wave acoustic field *J. Phys. A: Math. Gen.* **38** 3279

[31] Rogers G F C and Mayhew Y R 1985 *Thermodynamic and Transport Properties of Fluids* 3rd edn (London: Blackwell)